ROYAL SOCIETY
OF CHEMISTRY

PAPER

Facile one-pot synthesis of mulberry-shape silver nanoparticle-doped porphyrin nanoassembly with self-promoted electrochemiluminescence†

Yisha Wang, Jiangnan Shu,* Linfeng Zhuo, Manli Wang, Wei Nie and Hua Cui [iD] *

The electrochemiluminescence (ECL) efficiency of porphyrins is limited by the quenching of π–π stacking due to their poor water solubility and inherent instability. Therefore, there is an urgent need to design and explore novel porphyrin luminophores with high ECL efficiency, which presents a significant challenge. In this work, a facile one-pot strategy was developed to synthesize a self-promoter-doped porphyrin-based ECL luminophore with high ECL efficiency for the first time. The silver nanoparticle (AgNPs)-doped *meso*-tetra(4-carboxyphenyl) porphyrin (TCPP) (AgNPs@TCPP) nanoassembly was prepared by inducing TCPP assembly using Ag nanoseeds produced by the reduction of silver nitrate with N,N-dimethylformamide. In this process, AgNPs could coordinate with the carboxyphenyl groups at the terminus of TCPP and the pyrrole nitrogen of TCPP. The resulting AgNPs@TCPP nanoassembly demonstrated superior ECL performance using $K_2S_2O_8$ as a co-reactant, with an ECL efficiency of 217%, significantly higher than that of previously reported sodium dodecyl sulfate-assisted TCPP aggregate (92.3%) and cetyltrimethylammonium bromide-assisted TCPP aggregate (57.5%). The self-promoted and highly efficient ECL of the AgNPs@TCPP nanoassembly was attributed to overcoming the ECL quenching due to bad TCPP aggregation by virtue of Ag nanoseeds induced TCPP assembly and the self-promoted ECL amplification by doping AgNPs with excellent conductivity. These findings offer a new approach for exploring highly efficient porphyrin-based ECL luminophores, thereby expanding the applications of porphyrins in ECL.

Introduction

With the advantages of low background, simple operation, wide linear range and high sensitivity, electrochemiluminescence (ECL) has become the mainstream technology in clinical diagnosis.[1,2] The design and synthesis of efficient ECL luminophores are critical for ECL-based bioassays. A variety of ECL luminophores, such as organic compounds, metal complexes, metal oxides and nanomaterials, have been reported.[3] Notably, organic compounds have attracted great attention due to their good properties such as low toxicity, well-defined molecular structure, good biocompatibility and easy modification.[4]

Porphyrins are macromolecular heterocyclic compounds with a rigid planar structure, formed by linking the α-carbon atoms of four pyrrole subunits *via* a methine bridge.[5] As a class of organic ECL luminophores, porphyrins offer the advantages

of easy preparation and functionalization, tunable hydrophilicity/hydrophobicity and high luminescence efficiency. They have attracted increasing interest in ECL applications since the pioneering work of Bard and co-workers.[6] However, due to their poor solubility in water and inherent instability, porphyrins are prone to aggregation through π–π stacking interactions of the porphyrin ring in aqueous solutions. This aggregation could result in the occlusion of active sites within the porphyrin molecules and subsequent quenching of the ECL, thereby impeding the further advancement of porphyrins in the field of ECL.[7]

Up to now, various strategies have been proposed to address the above problems of porphyrins in ECL, which could be classified into two categories. The first approach involves the development of new porphyrin-based ECL luminophores through chemical bonding and the interplay of physical interactions.[7,8] For example, Zheng *et al.* encapsulated zinc(ɪɪ) *meso*-5,10,15,20-tetra(4-sulfonatophenyl)porphine in pyridyl-bridged β-cyclodextrin dimer, which underwent a compact self-assembly to form a clam-like inclusion complex with a 3-fold increase in ECL intensity.[9] Cai *et al.* utilized sodium dodecyl sulfate (SDS) as a "soft template" to synthesize a

Key Laboratory of Precision and Intelligent Chemistry, iChEM (Collaborative Innovation Center of Chemistry for Energy Materials), Department of Chemistry, University of Science and Technology of China, Hefei, Anhui 230026, P. R. China. E-mail: hcui@ustc.edu.cn, jiangnan@ustc.edu.cn

one-dimensional nanostructure of zinc 5,10,15,20-tetra(4-pyridyl)-21H,23H-porphine, which exhibited an enlarged reaction specific surface area and improved mass transfer ability, resulting in an amplified ECL signal.[10] The second approach is the development of auxiliary enhancement strategies such as self-enhancement, co-reaction promoter, oxygen participation and resonance energy transfer.[11–15] For example, Han et al. found that L-cysteine capped zinc oxide nanoflowers could accelerate the catalysis of potassium persulfate ($K_2S_2O_8$) to generate more sulfate radicals ($SO_4^{\bullet-}$), thereby resulting in an amplified ECL signal.[16] Li et al. proposed a novel ECL amplification system that integrated benzimidazole (BIM) and zinc(II) tetrakis(4-carboxyphenyl)porphine (ZnTCPP) into one framework based on the ECL resonance energy transfer.[17] On account of the overlapped spectra between the emission of BIM and the absorption of ZnTCPP, the energy of multiple BIM (donor) could be concentrated on a single ZnTCPP (acceptor), thereby amplifying the ECL emission of the acceptor. Although these progresses have expanded the applications of porphyrins in ECL, there is still a strong need for further improvements to enhance the ECL performance and efficiency of these porphyrin systems.

Herein, a strategy for the facile one-pot synthesis of self-promoter-doped porphyrin-based ECL luminophore was developed for the first time. Initially, silver nitrate ($AgNO_3$) was reduced to Ag nanoseeds by N,N-dimethylformamide (DMF) under sonication. Subsequently, a solution of meso-tetra(4-carboxyphenyl)-porphyrins (TCPP) was directly introduced to induce the assembly of the generated Ag nanoseeds. Following a growth period, silver nanoparticles (AgNPs)-doped TCPP (AgNPs@TCPP) nanoassembly with a mulberry shape was obtained. The successful formation of AgNPs@TCPP nanoassembly was confirmed by various techniques including scanning electron microscope (SEM), transmission electron microscopy (TEM), energy dispersive spectroscopy (EDS)-mapping, X-ray photoelectron spectroscopy (XPS), Fourier transform infrared spectroscopy (FT-IR) and UV-visible (UV-vis) absorption spectroscopy. Using $K_2S_2O_8$ as a co-reactant, the resulting AgNPs@TCPP nanoassembly exhibited highly efficient ECL emission. The related ECL mechanism investigated by cyclic voltammetry and electrochemical impedance spectroscopy (EIS) is proposed in detail.

Experimental

Chemicals and materials

$K_2S_2O_8$, $AgNO_3$, hexadecyl trimethyl ammonium bromide (CTAB), and SDS were purchased from Sinopharm Chemical Regent Co., Ltd (Shanghai, China). TCPP was purchased from J&K Scientific Ltd (Beijing, China). 0.01 M phosphate-buffered saline (PBS) buffer (pH 7.4) was purchased from Sangon Biotechnology Co., Ltd (Shanghai, China). All reagents were of analytical grade. Ultra-pure water (resistivity 18.2 MΩ cm, at 25 °C) was prepared using a Milli-Q system (Milli-pore, France) and used throughout. All glassware was cleaned with freshly prepared aqua regia, washed thoroughly in redistilled water, and dried prior to use.

Apparatus

Detailed information is described in the ESI,† Section S1.

Preparation of AgNPs@TCPP nanoassembly

First, 5 mg of $AgNO_3$ was dissolved in 5 mL of DMF by sonication for 2 min. Then, 5 mg of TCPP in 5 mL DMF was introduced and the reaction was allowed to proceed for 16 min at ambient temperature. Finally, the resulting sample was washed three times by centrifugation with DMF and ultrapure water to obtain the AgNPs@TCPP nanoassembly.

ECL measurements

A three-electrode system was built up by using a glassy carbon electrode (GCE) with a diameter of 5.0 mm as the working electrode, platinum wire as the counter electrode and Ag/AgCl (saturated KCl) electrode as the reference electrode to carry out ECL experiments. Alumina slurry (1.0, 0.3 and 0.05 μm) was used to polish the bare GCE on the polishing cloth followed by thorough rinsing with water, and sonication in ethanol and then rinsing again with distilled water. Then, 30 μL of AgNPs@TCPP nanoassembly was dropped onto the GCE and dried at 30 °C to form a uniform film. Finally, ECL measurements were performed in 0.01 M PBS buffer (pH 7.4) containing 0.02 M $K_2S_2O_8$ under cyclic voltammetric (CV) scan from 0 to −1.5 V (vs. Ag/AgCl) at a scan rate of 0.05 V s^{-1}. The high voltage of the photomultiplier tube (PMT) was −500 V. The three-dimensional (3D) ECL spectrum of AgNPs@TCPP nanoassembly was obtained using an ECL spectrum acquiring system described in the ESI,† Section S1. The ECL measurements were conducted in 0.01 M PBS buffer (pH 7.4) containing 0.02 M $K_2S_2O_8$ under CV from 0 to −1.8 V (vs. Ag/AgCl) at a scan rate of 0.05 V s^{-1}. Each spectrum was acquired for 1 s, with a time interval of 1 s.

Results and discussion

Synthesis and characterizations

The schematic illustration of the facile one-pot synthesis of AgNPs@TCPP nanoassembly is depicted in Fig. 1A. First, $AgNO_3$ was dissolved in DMF through sonication for 2 min. During this process, Ag^+ was reduced to Ag nanoseeds by DMF and the color of the solution changed from transparent to light yellow. Subsequently, TCPP solution was directly added, which induced the assembly of the generated Ag nanoseeds. Following a growth period, the AgNPs@TCPP nanoassembly was ultimately formed.

The successful synthesis of the AgNPs@TCPP nanoassembly was characterized by various methods including SEM, TEM, EDS-mapping, XPS, FT-IR and UV-vis absorption spectroscopy. The SEM image (Fig. 1B) revealed that the AgNPs@TCPP nanoassembly had dimensions of approximately 300 nm in length and 200 nm in width, with a mulberry shape. Additionally, the TEM image in Fig. 1C illustrated that AgNPs, with an average diameter of 9.68 ± 1.58 nm (Fig. S1, ESI†), were uniformly distributed within the TCPP nanoassembly. Moreover, the high-resolution TEM (HRTEM) image of AgNPs in the
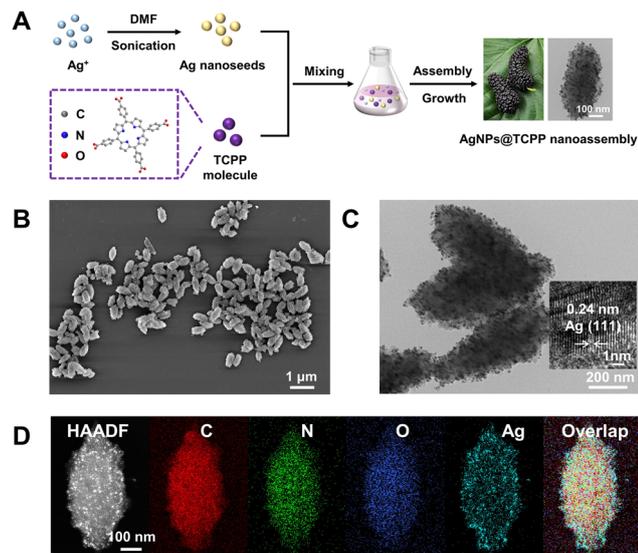
Fig. 1 (A) Schematic illustration for preparation of AgNPs@TCPP nanoassembly. (B) SEM image of AgNPs@TCPP nanoassembly. (C) TEM image of AgNPs@TCPP nanoassembly. Inset: HRTEM image of AgNPs in AgNPs@TCPP nanoassembly. (D) HAADF-STEM image of AgNPs@TCPP nanoassembly. EDS-mapping images of C, N, O and Ag elements and full element distribution of AgNPs@TCPP nanoassembly.
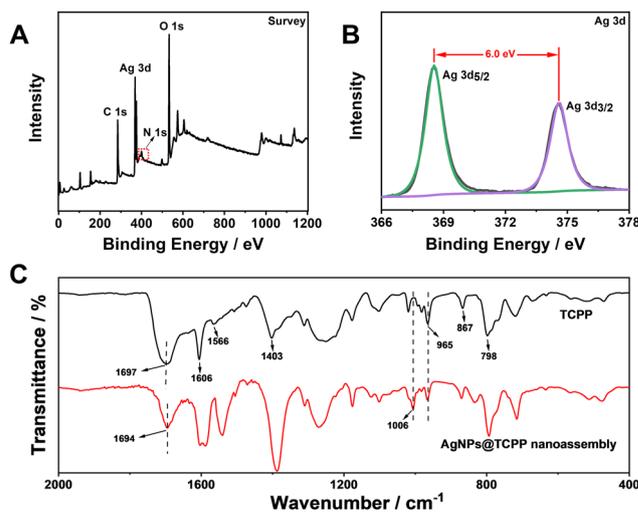

Fig. 2 (A) Survey XPS spectrum of AgNPs@TCPP nanoassembly. (B) Deconvolution XPS spectrum of Ag 3d in AgNPs@TCPP nanoassembly. (C) FT-IR spectra of TCPP (black curve) and AgNPs@TCPP nanoassembly (red curve).

AgNPs@TCPP nanoassembly (the inset of Fig. 1C) displayed a lattice spacing of 0.24 nm, corresponding to the (111) plane of the fcc Ag (JCPDS, No. 04-0783).[18,19] The selected area electron diffraction (SAED) ring pattern in Fig. S2 (ESI†) also indicated the polycrystalline nature of AgNPs, with diffraction rings indexed to (111), (200), (220) and (311), corresponding to the fcc crystal structure of metallic Ag.[20,21]

In addition, EDS-mapping measurements (Fig. 1D) confirmed the presence of C, N, O, and Ag elements within the AgNPs@TCPP nanoassembly, which was further supported by the survey XPS spectrum shown in Fig. 2A. Subsequently, the deconvoluted XPS spectrum of Ag 3d (Fig. 2B) revealed two peaks centered at 368.5 eV (Ag $3d_{5/2}$) and 374.5 eV (Ag $3d_{3/2}$), indicating the presence of Ag(0) in AgNPs@TCPP nanoassembly.[22,23] Furthermore, compared to the N 1s spectrum of TCPP (Fig. S3A, ESI†), a new deconvolution peak at around 398.5 eV appeared for the AgNPs@TCPP nanoassembly (Fig. S3B, ESI†). According to the literature, this peak was assigned to Ag–N, suggesting that AgNPs could coordinate with the pyrrole nitrogen of the TCPP.[24]

Besides, FT-IR spectra were recorded to study the functional groups and chemical structures of the synthesized AgNPs@TCPP nanoassembly. As with TCPP (Fig. 2C, black curve), the FT-IR spectrum of AgNPs@TCPP nanoassembly (Fig. 2C, red curve) exhibited the characteristic peaks for the big ring skeleton absorption (1606, 1566 and 1403 cm^{-1}) and benzene ring (867 and 798 cm^{-1}), indicating that AgNPs@TCPP nanoassembly maintained the pyrrole ring structure of TCPP.[25] Additionally, the characteristic peak of the carboxyl in TCPP shifted from 1697 cm^{-1} to 1694 cm^{-1} after the formation of AgNPs@TCPP nanoassembly, suggesting the coordination between the carbonyl of TCPP and AgNPs.[26] Moreover, the FT-IR spectrum of AgNPs@TCPP

nanoassembly (Fig. 2C, red curve) showed a decrease in the intensity of the characteristic peak at 965 cm^{-1}, representing the N-H telescopic vibration pattern on the pyrrole ring of TCPP, and the appearance of a new characteristic peak at 1006 cm^{-1}, representing the deformation vibration of the porphyrin ring. This further demonstrated that AgNPs could coordinate with the pyrrole nitrogen of TCPP.[27] In addition, the UV-vis absorption peaks at the AgNPs@TCPP nanoassembly (Fig. S4, red curve, ESI†) displayed absorption peaks at 415 and 448 nm, corresponding to the characteristic absorption of TCPP (Fig. S4, black curve, ESI†) and AgNPs, respectively, confirmed the existence of both TCPP and AgNPs in the nanoassembly.[28,29] These findings collectively indicated the successful preparation of the AgNPs@TCPP nanoassembly.

Formation mechanism of AgNPs@TCPP nanoassembly

In order to elucidate the formation mechanism of the AgNPs@TCPP nanoassembly, the UV-vis absorption spectrum of AgNO$_3$ in DMF was examined after sonication for 2 min. The result (Fig. S5, ESI†) demonstrated a characteristic peak at 422 nm, indicating the successful generation of Ag nanoseeds.[30] Then, the effects of AgNO$_3$ concentration and the growth time on the synthesis of AgNPs@TCPP nanoassembly were investigated. In the absence of AgNO$_3$, no product was obtained, indicating the essential role of AgNO$_3$ in the synthesis process. Furthermore, it was found that when the amount of the added AgNO$_3$ reached 5 mg, a sufficient number of Ag nanoseeds were present, leading to the formation of a mulberry-shaped AgNPs@TCPP nanoassembly with uniform morphology (Fig. S6B, ESI†). As illustrated in Fig. S6C and D (ESI†), the addition of higher amounts of AgNO$_3$ resulted in the appearance of numerous large AgNPs and rendered the nanoassembly unstable. Consequently, 5 mg of AgNO$_3$ was determined to be the optimal amount for the synthesis of the AgNPs@TCPP nanoassembly.

The results suggested that the generation of an adequate and appropriate amount of Ag nanoseeds was crucial for inducing the formation of morphologically uniform and stable TCPP assemblies. As presented in Fig. S7 (ESI†), the mulberry-shape AgNPs@TCPP nanoassemblies were gradually formed with increasing growth time, and their morphology was basically unchanged after 16 min. During the process, it was noted that the Ag nanoseeds grew into AgNPs and were doped within the TCPP nanoassembly. This result indicated that the AgNPs could rapidly induce TCPP for assembly, ultimately resulting in the formation of the AgNPs@TCPP nanoassembly. The synthesis time of the AgNPs@TCPP nanoassembly was found to be only 16 min, which was much shorter than the reported synthesis time of 48 h for the sodium dodecyl sulfate-assisted TCPP aggregate (SDS-TCPP aggregate) and cetyltrimethylammonium bromide-assisted TCPP aggregate (CTAB-TCPP aggregate).[31]

As a result, the formation mechanism of AgNPs@TCPP nanoassembly could be elucidated as follows. First, $AgNO_3$ was reduced by DMF under sonication, resulting in the formation of Ag nanoseeds. Subsequently, the Ag nanoseeds could induce the assembly of TCPP by coordinating with the carboxyphenyl groups at the terminus of TCPP and the pyrrole nitrogen of TCPP.[32–34] During the growth period, Ag nanoseeds grew into AgNPs and the TCPP nanoassembly underwent a morphological transformation into a mulberry-shaped structure with a homogeneous morphology. Finally, the mulberry-shape AgNPs@TCPP nanoassembly with a stable structure was successfully obtained.

Self-promoted ECL of AgNPs@TCPP nanoassembly

The ECL behavior of AgNPs@TCPP nanoassembly was investigated in 0.01 M PBS buffer with $K_2S_2O_8$ as a co-reactant using a CV scan between 0 to −1.50 V at a scan rate of 0.05 V s^{-1}. As shown in Fig. 3A, two intense ECL emissions (ECL-1 and ECL-2) were obtained in the ECL intensity–potential (I_{ECL}–E) curve of the AgNPs@TCPP nanoassembly. ECL-1 appeared at −0.62 V and reached the maximum intensity at −0.88 V, while ECL-2 started at an onset potential of −0.91 V and reached a maximum at −1.17 V. The CV curve was recorded simultaneously to highlight the ECL process. Three reduction peaks at −0.55 V (R1), −0.80 V (R2) and −1.28 V (R3) were observed (Fig. 3B, red curve) in the CV curve of the AgNPs@TCPP nanoassembly modified GCE in the presence of $K_2S_2O_8$. R1 was found to be assigned to the reduction of dissolved oxygen (O_2) as it also appeared in the CV curve of bare GCE in the absence of $K_2S_2O_8$ (Fig. 3B, purple curve). R2, which was also observed in the CV curve of the AgNPs@TCPP nanoassembly modified GCE without $K_2S_2O_8$ (Fig. 3B, green curve), was associated with the reduction of TCPP to TCPP$^{•-}$ according to the previous report.[35] Thus, corresponding to R2, the ECL-1 at −0.88 V was inferred to be related to the electro-reduction of TCPP in the AgNPs@TCPP nanoassembly. The black curve in Fig. 3B showed that $K_2S_2O_8$ could be reduced on the bare GCE at about −1.25 V. This suggested that R3 (−1.28 V), corresponding to ECL-2 (−1.17 V), was related to the electro-reduction of $K_2S_2O_8$ to produce $SO_4^{•-}$. As a result, ECL-1 and ECL-2 of the AgNPs@TCPP nanoassembly were associated with the electro-reduction of TCPP and $K_2S_2O_8$, respectively.
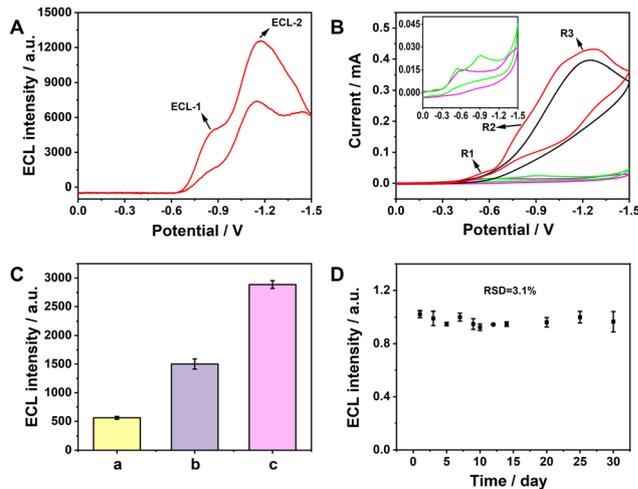

Fig. 3 (A) I_{ECL}–E curves of AgNPs@TCPP nanoassembly modified GCE in the presence of 0.02 M $K_2S_2O_8$. (B) CV curves of bare GCE in the presence (black curve) and absence (purple curve) of 0.02 M $K_2S_2O_8$ and AgNPs@TCPP nanoassembly modified GCE in the presence (red curve) and absence (green curve) of 0.02 M $K_2S_2O_8$. (C) ECL intensities of CTAB-TCPP aggregate (a), SDS-TCPP aggregate (b) and AgNPs@TCPP nanoassembly (c). (D) Inter-day ECL stability of AgNPs@TCPP nanoassembly. ECL was conducted in 0.01 M PBS buffer (pH 7.4) containing 0.02 M $K_2S_2O_8$, scan rate: 0.05 V s^{-1}, scan range: 0 to −1.5 V, PMT: −500 V.

To illustrate the high ECL efficiency of the AgNPs@TCPP nanoassembly, a comparison was made with the previously reported surfactant-assisted TCPP aggregates, specifically the SDS-TCPP aggregate and CTAB-TCPP aggregate. The synthesis and characterizations of the SDS-TCPP aggregate and the CTAB-TCPP aggregate are described in detail in the ESI,† Sections S9 and S10, and Fig. S8. As depicted in Fig. 3C, the ECL intensity of AgNPs@TCPP nanoassembly (Fig. 3C, c) was found to be 1.92 and 5.15 times higher than that of SDS-TCPP aggregate (Fig. 3C, b) and CTAB-TCPP aggregate (Fig. 3C, a), respectively, indicating the superior ECL performance of the prepared AgNPs@TCPP nanoassembly. Moreover, the ECL efficiencies of AgNPs@TCPP nanoassembly, SDS-TCPP aggregate and CTAB-TCPP aggregate with $K_2S_2O_8$ as a co-reactant were calculated and presented in Table S1 (ESI†), in which the $Ru(bpy)_3^{2+}/K_2S_2O_8$ system was used as a standard. An ECL efficiency of 217% was obtained for the AgNPs@TCPP nanoassembly, which was relatively higher than that of the SDS-TCPP aggregate (92.3%) and the CTAB-TCPP aggregate (57.5%). The result further demonstrated the high ECL efficiency of the AgNPs@TCPP nanoassembly.

To explore why the AgNPs@TCPP nanoassembly had such an excellent ECL performance, the CV curves of the AgNPs@TCPP nanoassembly modified GCE and the bare GCE in the presence of $K_2S_2O_8$ were analyzed. It was found that the reduction current of AgNPs@TCPP nanoassembly modified GCE (Fig. 3B, red curve) was obviously stronger than that of bare GCE (Fig. 3B, black curve), suggesting that the modification of AgNPs@TCPP nanoassembly could promote the electro-reduction of TCPP and $K_2S_2O_8$. Meanwhile, EIS was used to monitor the conductive property of the electrode interface. As displayed in Fig. S9 (ESI†), it demonstrated a substantial

decrease in the charge transfer resistance for the AgNPs@TCPP nanoassembly-modified GCE (red sign) compared to the TCPP-modified GCE (black sign). The result suggested that the doping of AgNPs with high conductivity improved the conductivity of the TCPP assembly, thereby facilitating electron transport and promoting the ECL processes. As a result, the self-promoted ECL of AgNPs@TCPP nanoassembly could be attributed to overcoming the ECL quenching due to bad TCPP aggregation by virtue of Ag nanoseed-induced TCPP assembly and the self-promoted ECL amplification by doping AgNPs with high conductivity.

Finally, the inter-day ECL stability of the AgNPs@TCPP nanoassembly was investigated. The data in Fig. 3D revealed a minimal relative standard deviation (RSD) of 3.1% in ECL intensity within 30 days. The result demonstrated the good ECL stability of the AgNPs@TCPP nanoassembly, suggesting its potential utility as an analytical interface or signal probe in bioassays.

ECL mechanism

To elucidate the ECL mechanism, a 3D ECL spectrum was obtained by recording the ECL intensity as a function of applied potential and emission wavelength using $K_2S_2O_8$ as a co-reactant in the potential range of 0 to -1.8 V. As shown in Fig. 4A, the ECL emission wavelength of the AgNPs@TCPP nanoassembly was located at 685 nm and remained constant throughout the CV scan. Furthermore, Fig. 4B shows that the ECL emission wavelength of the AgNPs@TCPP nanoassembly was basically consistent with that of the TCPP molecule, indicating that the ECL luminophore in the AgNPs@TCPP nanoassembly was TCPP. Then, the effects of $K_2S_2O_8$ concentration on the ECL intensity were studied. As shown in Fig. 4C, the ECL intensity increased with the increase of $K_2S_2O_8$ concentration and reached its maximum at 0.02 M $K_2S_2O_8$, while no ECL signal was observed in the absence of $K_2S_2O_8$. This phenomenon revealed the crucial role of $K_2S_2O_8$ in the formation of the ECL emissions. When the $K_2S_2O_8$ concentration exceeded 0.02 M, the ECL intensity decreased, possibly due to the quenching reaction between the excited-state species of TCPP (TCPP*) and $S_2O_8^{2-}$ according to the literature.[36] In addition, the effects of various atmospheres, including air, (nitrogen) N_2 and O_2 atmosphere, on the ECL emissions of the AgNPs@TCPP nanoassembly were also examined. As presented in Fig. 4D, the ECL intensity decreased significantly in the O_2-saturated atmosphere and showed no obvious change in the N_2-saturated atmosphere, suggesting that O_2 could quench the ECL emission of the AgNPs@TCPP nanoassembly. This might be due to the abundant hydroxyl radicals generated by electro-reduced O_2 being able to scavenge $SO_4^{\bullet-}$, thereby inhibiting the formation of the excited-state species of AgNPs@TCPP nanoassembly (AgNPs@TCPP*) and decreasing the ECL emission.[37–39]

Based on the aforementioned results, the possible ECL mechanism of the AgNPs@TCPP nanoassembly and $K_2S_2O_8$ system could be proposed as the following equations. At a lower potential, the AgNPs@TCPP nanoassembly could be electro-reduced to AgNPs@TCPP$^{\bullet-}$ (eqn (1)), which then reacted with $S_2O_8^{2-}$ to form $SO_4^{\bullet-}$ (eqn (2)). Subsequently, $SO_4^{\bullet-}$ reacted with AgNPs@TCPP$^{\bullet-}$ to generate AgNPs@TCPP*
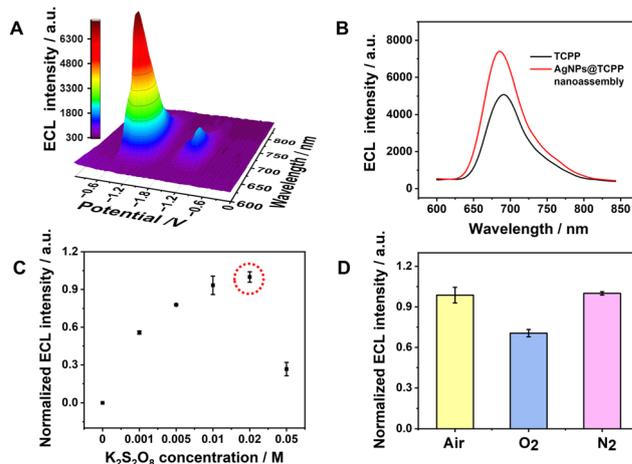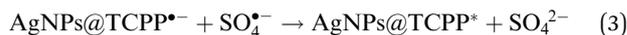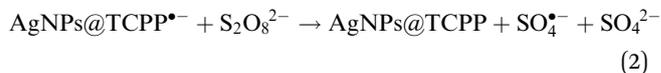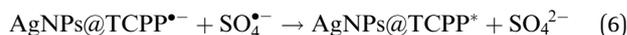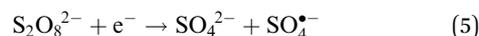

Fig. 4 (A) 3D ECL spectrum of AgNPs@TCPP nanoassembly. Each spectrum was acquired for 1 s with a time interval of 1 s. (B) ECL spectra of TCPP and AgNPs@TCPP nanoassembly. (C) Normalized ECL intensities of AgNPs@TCPP nanoassembly at different $K_2S_2O_8$ concentrations. (D) Normalized ECL intensities of AgNPs@TCPP nanoassembly at different atmospheres. ECL was conducted in 0.01 M PBS buffer (pH 7.4) containing 0.02 M $K_2S_2O_8$, scan rate: 0.05 V s^{-1}, scan range: 0 to -1.5 V, PMT: -500 V.

(eqn (3)), resulting in the ECL-1 emission at a potential of -0.88 V (eqn (4)). At a higher potential, $S_2O_8^{2-}$ could be directly electro-reduced to $SO_4^{\bullet-}$ (eqn (5)), which then reacted with AgNPs@TCPP$^{\bullet-}$ to produce AgNPs@TCPP* (eqn (6)), resulting in the ECL-2 emission at a potential of -1.17 V (eqn (7)). In addition, the doping of AgNPs in the AgNPs@TCPP nanoassembly could enhance the electron transfer at the electrode interface, thereby facilitating the aforementioned ECL processes and resulting in the self-promoted ECL emission.

ECL-1:

$$AgNPs@TCPP + e^- \rightarrow AgNPs@TCPP^{\bullet-} \qquad (1)$$

$$AgNPs@TCPP^{\bullet-} + S_2O_8^{2-} \rightarrow AgNPs@TCPP + SO_4^{\bullet-} + SO_4^{2-} \qquad (2)$$

$$AgNPs@TCPP^{\bullet-} + SO_4^{\bullet-} \rightarrow AgNPs@TCPP^* + SO_4^{2-} \qquad (3)$$

$$AGNPs@TCPP^* \rightarrow AgNPs@TCPP + h\nu \ (\lambda = 685 \text{ nm}) \qquad (4)$$

ECL-2:

$$S_2O_8^{2-} + e^- \rightarrow SO_4^{2-} + SO_4^{\bullet-} \qquad (5)$$

$$AgNPs@TCPP^{\bullet-} + SO_4^{\bullet-} \rightarrow AgNPs@TCPP^* + SO_4^{2-} \qquad (6)$$

$$AgNPs@TCPP^* \rightarrow AgNPs@TCPP + h\nu \ (\lambda = 685 \text{ nm}) \qquad (7)$$

Conclusions

In this work, a novel self-promoter-doped porphyrin-based ECL luminophore AgNPs@TCPP nanoassembly was synthesized by

a facile one-pot strategy. Initially, AgNO$_3$ was reduced by DMF to form Ag nanoseeds, which could then induce the assembly of TCPP by coordinating with the carboxyphenyl groups at the terminus of TCPP and the pyrrole nitrogen of TCPP. Finally, the mulberry-shaped AgNPs@TCPP nanoassembly was obtained after a short growth period of 16 min. Using K$_2$S$_2$O$_8$ as a co-reactant, the AgNPs@TCPP nanoassembly exhibited superior ECL performance with an ECL efficiency of 217%, which was significantly higher than that of the previously reported SDS-TCPP aggregate (92.3%) and the CTAB-TCPP aggregate (57.5%). The self-promoted and highly efficient ECL of AgNPs@TCPP nanoassembly was found to originate from overcoming the ECL quenching due to bad porphyrin aggregation by virtue of Ag nanoseed-induced TCPP assembly and the self-promoted ECL amplification by doping AgNPs with excellent conductivity. A related ECL mechanism is proposed. At a lower potential, AgNPs@TCPP$^{\bullet-}$ produced by electroreduction reacted with S$_2$O$_8^{2-}$ to form SO$_4^{\bullet-}$, which then reacted with AgNPs@TCPP$^{\bullet-}$ to generate AgNPs@TCPP*, resulting in the ECL-1 emission. At a higher potential, S$_2$O$_8^{2-}$ could be directly electro-reduced to SO$_4^{\bullet-}$, which then reacted with AgNPs@TCPP$^{\bullet-}$ to produce AgNPs@TCPP*, resulting in the ECL-2 emission. These findings provide a new route for the synthesis of highly efficient porphyrin-based ECL luminophores, which will advance the application of porphyrins in ECL.

Author contributions

Yisha Wang: conceived and designed the experiments, performed the experiments, data curation, investigation, methodology, writing-original draft. Jiangnan Shu: conceptualization, supervision, funding acquisition, writing-review and editing. Linfeng Zhuo: methodology. Manli Wang: data curation. Wei Nie: investigation. Hua Cui: conceptualization, funding acquisition, supervision, project administration, writing-review and editing.

Conflicts of interest

There are no conflicts to declare.

Acknowledgements

Notes and references

1 L. Li, Y. Chen and J.-J. Zhu, *Anal. Chem.*, 2016, **89**, 358–371.
2 Y. Chen, S. Zhou, L. Li and J.-J. Zhu, *Nano Today*, 2017, **12**, 98–115.
3 Z. Liu, W. Qi and G. Xu, *Chem. Soc. Rev.*, 2015, **44**, 3117–3142.
4 X. Zhang, P. Wang, Y. Nie and Q. Ma, *Trends Anal. Chem.*, 2021, **143**, 116410.
5 S. Ishihara, J. Labuta, W. Van Rossom, D. Ishikawa, K. Minami, J. P. Hill and K. Ariga, *Phys. Chem. Chem. Phys.*, 2014, **16**, 9713–9746.
6 Y. Xu, Z. Han, P. Du and X. Lu, *Trends Anal. Chem.*, 2023, **165**, 117136.
7 Y. Zhang, Y. Zhao, Z. Han, R. Zhang, P. Du, Y. Wu and X. Lu, *Angew. Chem., Int. Ed.*, 2020, **59**, 23261–23267.
8 Y. Zhou, J. He, C. Zhang, J. Li, X. Fu, W. Mao, W. Li and C. Yu, *ACS Appl. Mater. Interfaces*, 2019, **12**, 338–346.
9 C. Zheng, Y. Sheng, Y. Liu, Y. Wan, G. Liu, X. Zhang, M. Yang, K. Kang, J. Liu, K. Ma and S. Deng, *Anal. Bioanal. Chem.*, 2019, **411**, 4797–4806.
10 W.-R. Cai, G.-Y. Zhang, K.-K. Lu, H.-B. Zeng, S. Cosnier, X.-J. Zhang and D. Shan, *ACS Appl. Mater. Interfaces*, 2017, **9**, 20904–20912.
11 G. Pu, Z. Yang, Y. Wu, Z. Wang, Y. Deng, Y. Gao, Z. Zhang and X. Lu, *Anal. Chem.*, 2019, **91**, 2319–2328.
12 J. Ma, W. Wang, Y. Li, Z. Lu, X. Tan and H. Han, *Anal. Chem.*, 2021, **93**, 2090–2096.
13 Q. Han, C. Wang, P. Liu, G. Zhang, L. Song and Y. Fu, *Biosens. Bioelectron.*, 2021, **191**, 113422.
14 J. Lu, Y. Wang, X. Shan, Z. Sun, X. Zhang, Y. Zhao, Y. Hu, E. Sun and L. Tian, *Microchem. J.*, 2021, **170**, 106716.
15 S. Deng, T. Zhang, X. Ji, Y. Wan, P. Xin, D. Shan and X. Zhang, *Anal. Chem.*, 2015, **87**, 9155–9162.
16 Q. Han, C. Wang, Z. Li, J. Wu, P. K. Liu, F. Mo and Y. Fu, *Anal. Chem.*, 2020, **92**, 3324–3331.
17 Y.-X. Li, J. Li, H.-B. Zeng, X.-J. Zhang, S. Cosnier and D. Shan, *Anal. Chem.*, 2023, **95**, 3493–3498.
18 H. Zhu, M. Du, M. Zhang, P. Wang, S. Bao, L. Wang, Y. Fu and J. Yao, *Biosens. Bioelectron.*, 2013, **49**, 210–215.
19 Q. Lu, J. Deng, Y. Hou, H. Wang, H. Li, Y. Zhang and S. Yao, *Chem. Commun.*, 2015, **51**, 7164–7167.
20 D. Garibo, H. A. Borbón-Nuñez, J. N. D. de León, E. García Mendoza, I. Estrada, Y. Toledano-Magaña, H. Tiznado, M. Ovalle-Marroquin, A. G. Soto-Ramos, A. Blanco, J. A. Rodríguez, O. A. Romo, L. A. Chávez-Almazán and A. Susarrey-Arce, *Sci. Rep.*, 2020, **10**, 12805.
21 E. Murugan, S. Santhosh Kumar, K. M. Reshna and S. Govindaraju, *J. Mater. Sci.*, 2018, **54**, 5294–5310.
22 J. Qin and H. Zeng, *Appl. Catal., B*, 2017, **209**, 161–173.
23 T. Gan, Z. Lv, J. Sun, Z. Shi and Y. Liu, *J. Hazard. Mater.*, 2016, **302**, 188–197.
24 N. Maiti, S. Thomas, A. Debnath and S. Kapoor, *RSC Adv.*, 2016, **6**, 56406–56411.
25 L. Cui, J. Wu, J. Li and H. Ju, *Anal. Chem.*, 2015, **87**, 10635–10641.
26 M. Yan, J. Ye, Q. Zhu, L. Zhu, J. Huang and X. Yang, *Anal. Chem.*, 2019, **91**, 10156–10163.
27 S. Li, Y. Guo, L. Liu, J. Wang, L. Zhang, W. Shi, M. Aleksandrzak, X. Chen and J. Liu, *Catalysts*, 2023, **13**, 732.
28 R. M. Gengan, K. Anand, A. Phulukdaree and A. Chuturgoon, *Colloids Surf., B*, 2013, **105**, 87–91.

29 H. He, G. Tao, Y. Wang, R. Cai, P. Guo, L. Chen, H. Zuo, P. Zhao and Q. Xia, *Mater. Sci. Eng., C*, 2017, **80**, 509–516.

30 R. He, X. Qian, J. Yin and Z. Zhu, *J. Mater. Chem.*, 2002, **12**, 3783–3786.

31 Q. Han, C. Wang, Z. Li, J. Wu,P., K. Liu,F. Mo and Y. Fu, *Anal. Chem.*, 2020, **92**, 3324–3331.

32 L. Cui, M.-h Zhao, C.-c Li, Q. Wang, X. Luo and C.-y Zhang, *Anal. Chem.*, 2021, **93**, 2974–2981.

33 J. Li, L. Qu, H. Li, L. Zhao, T. Chen, J. Liu, Y. Gao and H. Pan, *Microchim. Acta*, 2023, **190**, 366.

34 D. E. Nevonen, J. C. Wagner, C. Brückner, C. J. Ziegler and V. N. Nemykin, *J. Phys. Chem. Lett.*, 2023, **14**, 7382–7388.

35 D. Luo, B. Huang, L. Wang, A. M. Idris, S. Wang and X. Lu, *Electrochim. Acta*, 2015, **151**, 42–49.

36 J. Li, N. Wang, T. Tran, T. C. A. Huang, L. Chen, L. Yuan, L. Zhou, R. Shen and Q. Cai, *Analyst*, 2013, **138**, 2038–2043.

37 B. Wang, G. Wang, J. Li, X. Liu, N. Ni, H. Su, M. Chen and L. Mao, *Small*, 2022, **19**, 2205607.

38 P.-P. Dai, T. Yu, H.-W. Shi, J.-J. Xu and H.-Y. Chen, *Anal. Chem.*, 2015, **87**, 12372–12379.

39 C. Wang, Z. Li and H. Ju, *Anal. Chem.*, 2021, **93**, 14878–14884.